Available online at www.sciencedirect.com
ScienceDirect
C. R. Physique 9 (2008) 119–126
COMPTES RENDUS PHYSIQUE
http://france.elsevier.com/direct/COMREN/

Physics/Atoms, molecules

SPROM – an efficient program for NMR/MRI simulations of inter- and intra-molecular multiple quantum coherences

Congbo Cai [a], Meijin Lin [a], Zhong Chen [a,b,*], Xi Chen [a], Shuhui Cai [a], Jianhui Zhong [b]

[a] *Departments of Physics and Communications Engineering, State Key Laboratory of Physical Chemistry of Solid Surface, Xiamen University, Xiamen 361005, China*

[b] *Department of Radiology, University of Rochester, Rochester, NY 14642, USA*

Received 14 April 2007; accepted after revision 6 November 2007

Presented by Jacques Villain

Abstract

A software package has been designed to simulate nuclear magnetic resonance spectra and images. Combining the product operator matrix with the non-linear Bloch equations, the software can efficiently simulate classical and quantum effects including scalar coupling, dipolar coupling, translational diffusion, chemical shift, radiation damping, transverse relaxation, and longitudinal relaxation. One of the most unique features of the software is its ability to incorporate effects of inter- and intra-molecular multiple quantum coherences in complex multiple-spin coupled systems, which are difficult with other existing software packages. The software, written in Visual C++, has a friendly graphical user interface and is easy to use. ***To cite this article: C. Cai et al., C. R. Physique 9 (2008).***

Résumé

SPROM – Un programme performant pour les simulations RMN/IRM de cohérences quantiques multiples inter- et intra-moléculaires. Un progiciel a été développé pour simuler les spectres et les images de résonnance magnétique nucléaire. Combinant la matrice opérateur de produit et les équations de Bloch non-linéaires, le logiciel simule efficacement les effets classiques et quantiques, notamment le couplage scalaire, le couplage dipolaire, la diffusion translationnelle, le décalage chimique, l'amortissement radiatif, la relaxation transverse et la relaxation longitudinale. Un des aspects les plus originaux de ce logiciel est sa capacité à incorporer les effets de cohérences quantiques multiples inter- et intra-moléculaire dans les systèmes complexes de spins multiples couplés, ce qui est difficile avec les progiciels existants. Doté d'une interface graphique conviviale, lee logiciel, écrit en Visual C++, est facile d'utilisation. ***Pour citer cet article : C. Cai et al., C. R. Physique 9 (2008).***

Keywords: Simulation software; Product operator matrix; Nuclear magnetic resonance; Magnetic resonance imaging; Inter- and intra-molecular multiple-quantum coherences

Mots-clés : Progiciel de simulation ; Matrice opérateur de produit ; Résonnance magnétique nucléaire ; Imagerie de résonnance magnétique ; Cohérences quantiques multiples inter- et intra-moléculaire

* Corresponding author.
E-mail address: chenz@xmu.edu.cn (Z. Chen).

1631-0705/$ – see front matter
doi:10.1016/j.crhy.2007.11.007

1. Introduction

Numerical simulation is powerful in handling complicated systems for which analytical methods are excluded or difficult to follow [1–3]. Nuclear magnetic resonance (NMR) spectra and magnetic resonance imaging (MRI) resulting from complex pulse sequences can be predicted by computer simulations before experiments [4,5]. Computer simulations provide guidance for selecting proper experimental parameters for optimal results and reduced experimental times [6–9]. Furthermore, they may help to identify the potential problems occurring in experiments when experimental results are not in agreement with theoretical predictions.

In spin dynamic calculations, macroscopic effects of relaxation, molecular diffusion, chemical shift, inhomogeneous magnetic field, radiation damping field, and long-range dipolar field can all be incorporated in the Bloch equations [10]. These equations play an important role in NMR studies [11], but they fail when scalar couplings, which are microscopic quantum effects, exist in spin systems as well. On the other hand, the density matrix formalism can be used to deal with complex quantum-mechanical behavior of an ensemble of spins [12], but it cannot handle macroscopic effects such as radiation damping, diffusion, and relaxations.

In the past quite a few simulation software packages have been developed, including BlochLib [13], Qsim [14], among many others. However, none of them can conveniently and efficiently simulate macroscopic and quantum effects at the same time. To fill this gap, a simulation package is introduced in this Note, which we dub Simulation with PRoduct Operator Matrix or SPROM. By adopting the PRoduct Operator Matrix (PROM), M_{mat}, to describe scalar couplings among multiple spins, the SPROM program can deal with scalar couplings in the framework of the non-linear Bloch equations [15]. The program is written in Visual C++ and provides a friendly graphical user interface (GUI). Preliminary tests show that the program is convenient and efficient at simulating several different effects in liquid spin-1/2 NMR and MRI experiments [16–19].

2. Theories and algorithms

2.1. Dynamical equations

Deville first introduced the concept of classical dipolar field, and proposed the non-linear Bloch equations with an additional dipolar field term [20]. After that, Jeener proposed an iterative scheme for solving the modified Bloch–Redfield equations or Torrey's equations [21]. If the superscript i represents the i-th type of spin, the motion equation of the magnetization vector $\boldsymbol{M}^{(i)}(\boldsymbol{r},t)$ in a frame rotating at the Larmor frequency is given by:

$$\frac{d\boldsymbol{M}^{(i)}(\boldsymbol{r},t)}{dt} = \gamma \boldsymbol{M}^{(i)}(\boldsymbol{r},t) \times \left\{ \frac{\omega_i}{\gamma}\hat{\boldsymbol{z}} + \boldsymbol{G}(\hat{\boldsymbol{s}},\boldsymbol{r})z + \Delta\boldsymbol{B}(\boldsymbol{r},t) + \sum_j \left[\boldsymbol{B}_r^{(j)}(\boldsymbol{r},t) + \boldsymbol{B}_d^{(j)}(\boldsymbol{r},t)\right] \right\} - \frac{M_x^{(i)}(\boldsymbol{r},t)\hat{\boldsymbol{x}} - M_y^{(i)}(\boldsymbol{r},t)\hat{\boldsymbol{y}}}{T_2^{(i)}(\boldsymbol{r})} + \frac{M_0^{(i)}\hat{\boldsymbol{z}} - M_z^{(i)}(\boldsymbol{r},t)\hat{\boldsymbol{z}}}{T_1^{(i)}(\boldsymbol{r})} + D_T^{(i)}\nabla^2\boldsymbol{M}^{(i)}(\boldsymbol{r},t) \tag{1}$$

where γ is the magnetogyric ratio; $\hat{\boldsymbol{x}}$, $\hat{\boldsymbol{y}}$, and $\hat{\boldsymbol{z}}$ are unit vectors along three orthogonal coordinate axes; $\hat{\boldsymbol{s}}$ is a unit vector along the direction of the gradient applied for modulating the dipolar field, and $G(\hat{\boldsymbol{s}},\boldsymbol{r})$ is the strength of this gradient along the $\hat{\boldsymbol{s}}$ direction at position $\boldsymbol{r}$; $\Delta\boldsymbol{B}(\boldsymbol{r},t)$ is the inhomogeneous field at position $\boldsymbol{r}$; $D_T^{(i)}$, $T_1^{(i)}$ and $T_2^{(i)}$ are the translational self-diffusion coefficient, longitudinal relaxation time, and transverse relaxation time of the i-th type of spins, respectively. ω_i is the frequency offset of the i-th type of spins; $M_x^{(i)}(\boldsymbol{r},t)$, $M_y^{(i)}(\boldsymbol{r},t)$ and $M_z^{(i)}(\boldsymbol{r},t)$ are the x, y and z components of $\boldsymbol{M}^{(i)}(\boldsymbol{r},t)$; $M_0^{(i)}\hat{\boldsymbol{z}} = M^{(i)}(\boldsymbol{r},0)$ is the initial magnetization vector of the i-th type of spins, and $\boldsymbol{B}_r^{(j)}(\boldsymbol{r},t)$ and $\boldsymbol{B}_d^{(j)}(\boldsymbol{r},t)$ are the radiation damping field and dipolar field of the j-th type of spins, respectively. $\boldsymbol{B}_r^{(j)}(\boldsymbol{r},t)$ is given by [22]:

$$\boldsymbol{B}_r^{(j)}(\boldsymbol{r},t) = \frac{\langle M_y^{(j)}(t)\rangle}{\gamma M_0^{(j)}\tau_r^{(j)}}\hat{\boldsymbol{x}} + \frac{\langle M_x^{(j)}(t)\rangle}{\gamma M_0^{(j)}\tau_r^{(j)}}\hat{\boldsymbol{y}} \tag{2}$$

where $\tau_r^{(j)} = 1/(2\pi\eta M_0^{(j)} Q\gamma)$ is the characteristic time of radiation damping, η is the filling factor, Q is the probe Q-factor, and $\langle M_x^{(j)}(t)\rangle$ and $\langle M_y^{(j)}(t)\rangle$ are the average magnetizations along the x and y directions respectively. The detailed calculation method of $\boldsymbol{B}_d^{(j)}(\boldsymbol{r}, t)$ can be found in Refs. [15,16].

Eq. (1) is a set of differential equations involving partial derivatives. In order to describe the detected NMR signal at time t_{final}, it must be integrated from $t = 0$ to t_{final}, which was done with a fifth-order Cash–Karp Runge–Kutta formalism [22] in this work.

2.2. Product operator matrix

PROM is a subset of the density matrix, which is simple and efficient for studying complex multi-spin-1/2 systems [15]. If I and S represent two kinds of spins scalar coupled with each other, a PROM of the $I_n S_m$ spin-1/2 system can be built with a $\underbrace{4 \times 4 \times \cdots \times 4}_{n+m}$ coherence matrix, where n and m are the numbers of I and S spins respectively. The element of the PROM is represented by $M_{\text{mat}}(L_{1a}, L_{2a}, \ldots, L_{ia}, \ldots, L_{(n+m)a})$, where L_{ia} represents a specific component (such as I_{ix}, I_{iy}, I_{iz}, or S_{ix}, S_{iy}, S_{iz}) of the i-th spin operator or unit element E. Since the base operator, $2^{q-1} I_{1a} I_{2a} \cdots I_{na} S_{1a} S_{2a} \cdots S_{ma}$, corresponds to a coherence term, where q is the number of spin operators in the product operator, $M_{\text{mat}}(L_{1a}, L_{2a}, \ldots, L_{ia}, \ldots, L_{(n+m)a})$ can be considered as the magnitude of the base operator. For example, $M_{\text{mat}}(I_{1x}, I_{2x}, \ldots, I_{nx}, S_{1x}, \ldots, S_{mx})$ represent the magnitude of coherence term $2^{n+m-1} I_{1x} I_{2x} \cdots I_{nx} S_{1x} S_{2x} \cdots S_{mx}$, and $M_{\text{mat}}(I_{1x}, E, \ldots, E, \ldots, E)$ represents the intensity value of I_{1x} term. The elements of the product operator matrix corresponding to I_{ix}, I_{iy}, and I_{iz} (or S_{ix}, S_{iy}, and S_{iz}) can be treated as specific components of a general 'magnetization vector' $\boldsymbol{M}^{(i)}$. The evolution of $\boldsymbol{M}^{(i)}$ under chemical shift, RF field, inhomogeneous background field, dipolar field, radiation damping, and diffusion can be described by the modified Bloch equations shown in Eq. (1). Relaxation is not included except for the single-quantum term due to the complexity of relaxation in the case of intra-molecular MQCs [23]. Scalar couplings are independently introduced into the PROM. According to the properties of scalar couplings, four matrix operation rules can be deduced:

$$\left.\begin{aligned}
&M_{\text{mat}}(I_{1a}, I_{2a}, \ldots, E, \ldots, I_{na}, S_{1a}, S_{2a}, \ldots, S_{jx}, \ldots, S_{ma}) \overset{2I_{iz}S_{jz}}{\longleftrightarrow} M_{\text{mat}}(I_{1a}, I_{2a}, \ldots, I_{iz}, \ldots, I_{na}, S_{1a}, S_{2a}, \ldots, S_{jy}, \ldots, S_{ma})\\
&M_{\text{mat}}(I_{1a}, I_{2a}, \ldots, E, \ldots, I_{na}, S_{1a}, S_{2a}, \ldots, S_{jy}, \ldots, S_{ma}) \overset{2I_{iz}S_{jz}}{\longleftrightarrow} M_{\text{mat}}(I_{1a}, I_{2a}, \ldots, I_{iz}, \ldots, I_{na}, S_{1a}, S_{2a}, \ldots, S_{jx}, \ldots, S_{ma})\\
&M_{\text{mat}}(I_{1a}, I_{2a}, \ldots, I_{ix}, \ldots, I_{na}, S_{1a}, S_{2a}, \ldots, E, \ldots, S_{ma}) \overset{2I_{iz}S_{jz}}{\longleftrightarrow} M_{\text{mat}}(I_{1a}, I_{2a}, \ldots, I_{iy}, \ldots, I_{na}, S_{1a}, S_{2a}, \ldots, S_{jz}, \ldots, S_{ma})\\
&M_{\text{mat}}(I_{1a}, I_{2a}, \ldots, I_{iy}, \ldots, I_{na}, S_{1a}, S_{2a}, \ldots, E, \ldots, S_{ma}) \overset{2I_{iz}S_{jz}}{\longleftrightarrow} M_{\text{mat}}(I_{1a}, I_{2a}, \ldots, I_{ix}, \ldots, I_{na}, S_{1a}, S_{2a}, \ldots, S_{jz}, \ldots, S_{ma})
\end{aligned}\right\} \quad (3)$$

Eq. (3) provides the evolution behavior of the matrix elements due to the scalar coupling operator $2I_{iz}S_{jz}$. Similar coherence matrixes and scalar coupling processes can be obtained for different weakly coupled systems such as AMX spin-1/2 system. More detailed descriptions can be found in our previous paper [15].

2.3. Diffusion simulation

Eq. (1) includes a diffusion term of $D_T^{(i)} \nabla^2 \boldsymbol{M}^{(i)}(\boldsymbol{r}, t)$. SPROM provides three kinds of numerical methods for simulations of diffusion: Torrey's method (solving directly the non-linear Bloch equations) [22], Monte Carlo method [24], and finite difference method [25].

For the Torrey's method, the diffusion term in Eq. (1) was treated in Fourier transformation space to reduce the computing time. Since the calculation of the bulk diffusion operator $D_T^{(i)}\nabla^2$ is reduced to multiplication $-D_T^{(i)}k^2$ in Fourier space, the Torrey's method is usually used in the situation where the dipolar field cannot be localized. In the case of 'anomalous diffusion' where molecular displacements during successive time intervals are correlated, the Torrey's method (diffusion operator $D_T^{(i)}\nabla^2$) does not work [26].

The Monte Carlo method is most flexible and intuitive, but most time-consuming for complex spin systems under multiple pulse sequences. It was used in some special cases reported previously [24].

Compared to the Monte Carlo method, the finite difference method can save computing time substantially and has higher precision in normal NMR simulations. A simple equation of finite difference method for 1D diffusion implemented in SPROM can be expressed as [27]

$$M_j^{n+1} = M_j^n + D_{j-1,j}\frac{\Delta t}{\Delta x^2}\left(M_{j-1}^n - M_j^n\right) + D_{j,j+1}\frac{\Delta t}{\Delta x^2}\left(M_{j+1}^n - M_j^n\right) \tag{4}$$

where M_j^n is the magnetization at the j-th position along a special axis and at the n-th time step; $D_{j,j+1}$represents the effective diffusion coefficient between the j-th and $(j+1)$-th element. In the implemented finite difference method in SPROM, every element of the PROM was operated directly through Eq. (4), with M_j^n replaced by M_{mat} [16].

2.4. Overview of the calculations

In this section, only the part of the calculation related to PROM is described. In the simulation, PROM is evolved until the simulation is completed. At each step, dipolar field is calculated first through the magnetization vector obtained from the PROM. The PROM is then evolved under the effects of chemical shift, relaxation, radiation damping, and dipolar coupling implemented in a fifth-order Cash–Karp Runge–Kutta formalism. The effect of diffusion is calculated independently by finite difference method or incorporated in the non-linear Bloch equations. Finally, PROM is evolved under the effects of scalar coupling by Eq. (3).

3. Basic features and settings

3.1. Basic features

The SPROM was developed with Visual C++ development tools (Microsoft, WA, USA). It can be run as a standalone application in any personal computer (PC) with Microsoft Windows operation system (Windows 2000 or later). All operations of SPROM are performed via an easy-to-use GUI similar to general Windows application programs. Since the core calculation code is written in standard C code, it is easy to parallelize or translate to other operation systems.

The main functions of SPROM include: (1) simulation of 1D and 2D spectra of the $I_n S_m$ (or ABX) spin-1/2 system in solution NMR, (2) simulation of MR images in coupled spin systems, and (3) input and output graphical interface. Fig. 1 provides examples of two designed pulse sequences and the corresponding sequence diagrams output from the SPROM software.

To begin a simulation, one first inputs spectral parameters and defines spin systems, then constructs pulse sequences. Outcomes of the simulation will then be presented as spectra or images. The whole process is intuitive and simple.

3.2. Spin system parameters

All spin system parameters such as the equilibrium magnetization intensity M_0, gyromagnetic ratio γ, chemical shifts ω, longitudinal relaxation time T_1, transverse relaxation time T_2, translational self-diffusion coefficient D, and scalar coupling constants J, can be assigned in the software package. The number of simulated spin systems is not limited. It only depends on your demand and computing time allowed, since a system with a large number of spins requires longer computing time.

3.3. Pulse sequences

After the spin system parameters are input, a pulse sequence needs to be constructed. A pulse sequence design is put under three basic components in SPROM: 'RF Pulse', 'Evolution', and 'Acquisition'. Flip angle, duration and phase, saturation pulse, related gradient strength, and frequency offset of a RF pulse can all be set under 'RF pulse' space. Free evolution or gradient pulse can be set under 'Evolution' space. A pulse sequence ends with 'Acquisition' space, in which the receiver phase can be set. SPROM can easily implement three advanced performances: phase cycling, multi-tasks, and batch processing.

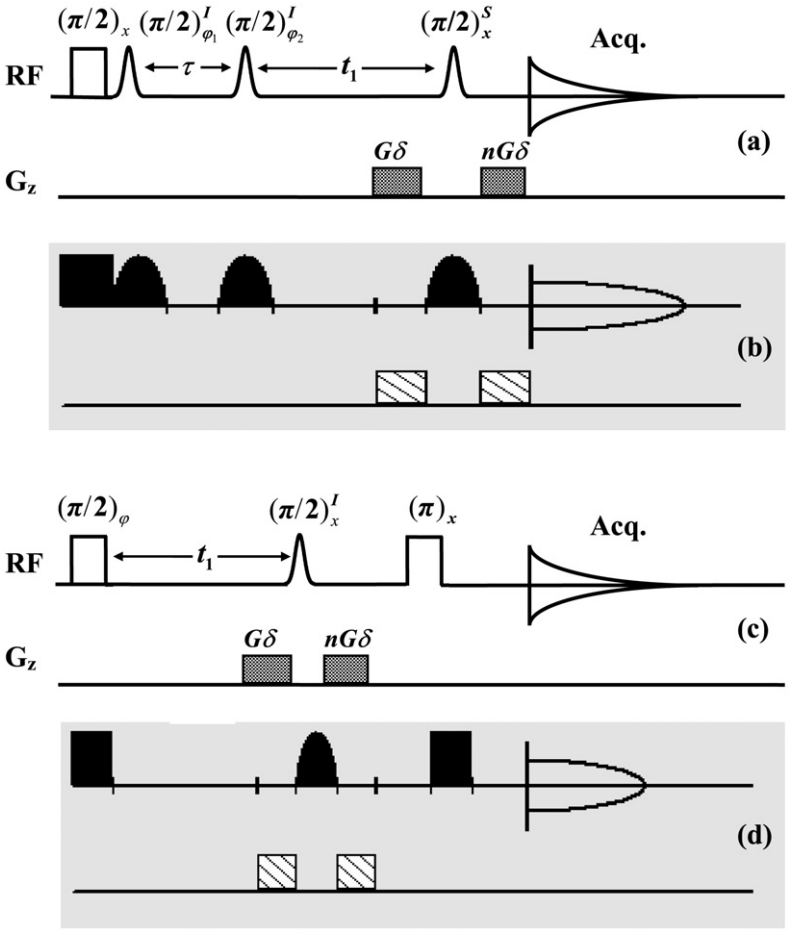

Fig. 1. (a) Pulse sequence for selecting intra- and inter-molecular MQC signals. The first RF pulse is non-selective, and the other three RF pulses are frequency-selective for I, I, and S spins respectively; (b) Diagram of the pulse sequence in (a) given by the SPROM software; (c) Pulse sequence for inter-molecular MQC signal in magnetic resonance imaging. The second RF pulse is selective for I and the others are non-selective (spatially selecting gradients were omitted for clarity); (d) Diagram of the pulse sequence in (c) given by the SPROM software.

3.4. Drawing results

Once the simulation is completed, the results can be drawn by SPROM software. These results include general 2D spectra, 1D spectra, array spectra, and gray-scale images. SPROM software provides three types of map for 2D spectra: gray map, color map and contour map. 2D spectra can be rotated by any angle. This function is especially useful for high-resolution intermolecular multiple-quantum coherence (MQC) 2D spectra in inhomogeneous field. The project of 2D spectrum along the direct and indirect dimensions can also be performed.

4. Simulation examples

To demonstrate the feasibility of the SPROM program, some NMR spectra were simulated for a 500 MHz NMR spectrometer, as given in Fig. 2. The sample is $CHCl_2CH_2Cl$ (IS_2 spin system) solution in acetone-D_6, where the protons in –CH and –CH_2 are denoted as I and S respectively. The scalar coupling constant between spins I and S is 5.8 Hz. The sample concentration is $M_0^{\mathrm{IS}} = 0.015$ A/m, and the effects of the radiation damping were neglected. The pulse sequence shown in Fig. 1(a) with $n = -2$ was used. Fig. 2 shows that the inter-molecular double-quantum coherence (DQC) cross-peak from I spins is a quartet with intensity ratio of 1:3:3:1 along the F_1 axis and a triplet with intensity ratio of 1:2:1 along the F_2 axis, while the signal from S spins is a doublet with intensity ratio of 1:1

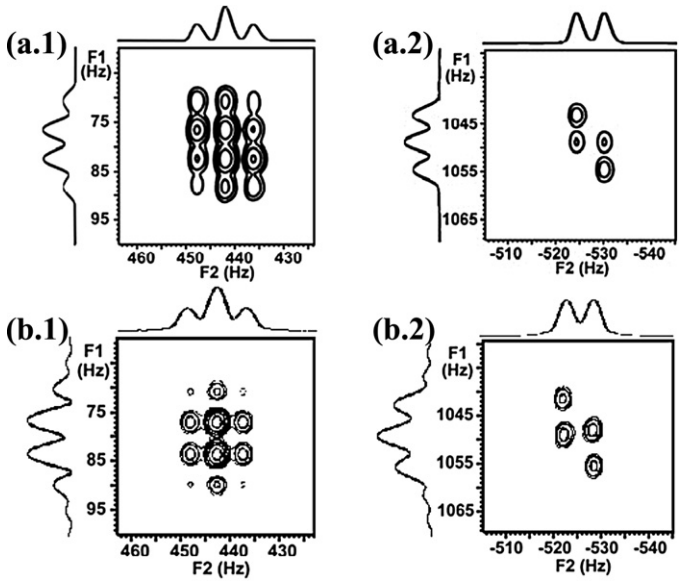

Fig. 2. Expansions of experimental (a) and simulated (b) 2D DQC spectra of $CHCl_2CH_2Cl$ sample from pulse sequence of Fig. 2(a) when $\tau = 1/J$ m s. (a.1) and (b.1) are signals of I spins, and (a.2) and (b.2) are signals of S spins.

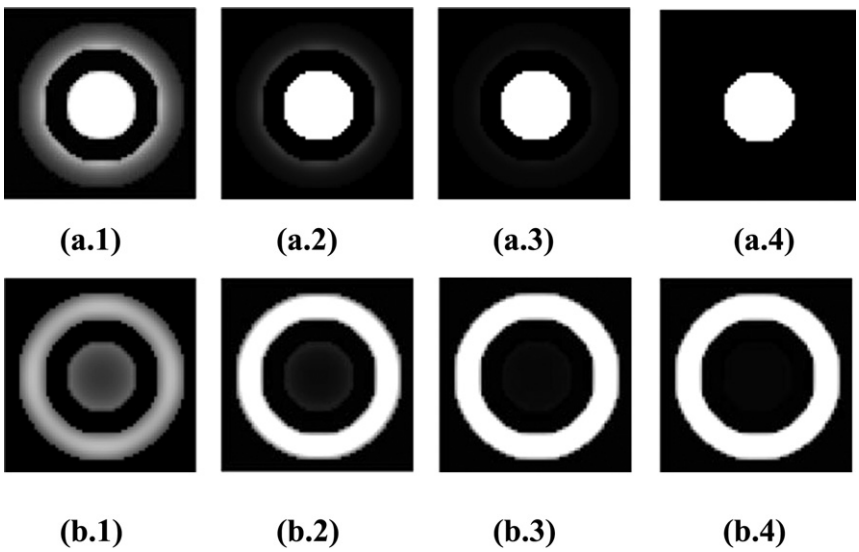

Fig. 3. Simulated images of a sample with two concentric tubes. The pulse sequence shown in Fig. 1(c) with $n = -2$ was used with different dipolar correlation distance r_d. The inner tube contains c_1 spin system (0.353 mm id, 0.561 mm od) and the outer tube contains c_2 spin system (0.820 mm id). For (a), c_1 represents I spins and c_2 represents S spins, for (b), c_1 represents S spins and c_2 represents I spins. (1) $r_d = 1.280$ mm, (2) $r_d = 0.588$ mm, (3) $r_d = 0.294$ mm, (4) $r_d = 0.196$ m.

along the F_2 axis and a doublet with intensity ratio of 1:1 along the diagonal. The complex splitting patterns were caused by the joint effects of the inter- and intra-molecular DQCs. In the case, theoretical deduction for the analytical signal expression is very convoluted, while the simulation result is much intuitive. The simulated results are in good agreement with experimental observations.

MRI has been under development over the past two decades and has become one of the most widely used medical imaging modalities [28]. The roles of dipolar coupling between distant spins in water and tissues were realized more recently, and a wealth of their possible applications has emerged [29,30]. In Fig. 3, a sample with two concentric tubes containing spins I ($\omega_I = 0$ Hz) and S ($\omega_S = 55$ Hz) respectively was tested. The inner and outer diameters of

the inner tube were 0.353 mm and 0.561 mm, respectively. For Fig. 3(a), the inner tube contained spins I and the outer tube contained spins S. For Fig. 3(b), physical locations of I and S were interchanged relative to Fig. 3(a). The other parameters were: $T_1 = 2$ s, $T_2 = 1$ s, and diffusion coefficient $D = 2.0 \times 10^{-9}$ m^2 s^{-1} for both spins. The pulse sequence shown in Fig. 1(c) with $n = -2$ was used. A simple phase cycle $(x, y, -x, -y)$ was applied to the first $\pi/2$ RF pulse, along with a receiver phase cycle $(x, -x, x, -x)$. Fig. 3(a) shows that in the region of the outer tube, the intensity of the image signal decreases with reduction of the dipolar correlation distance r_d, and the signal is mainly concentrated in the region closed to the inner tube. The reduction of signal intensity in the outer tube is due to reduction of the strength of the dipolar field produced in the inner tube. When r_d is smaller than the wall thickness of the inner tube, there is almost no signal in the region of the outer tube. These results indicate that the effects of inter-molecular dipolar couplings can cross the wall of tube with an effective range decided by the dipolar correlation distance. Similar conclusions can be extracted from Fig. 3(b), coincident with Ref. [31].

All above simulations were performed on a PC (AMD XP 2500+, 512MB memories). The computing time varied from several minutes to several hours, depending on the complexity of the spin systems and pulse sequences.

5. Conclusion

In conclusion, SPROM is a powerful and efficient tool for simulating classical and quantum effects in solution NMR and MRI. It can be applied to complex weakly-coupled spin-1/2 systems under the effects of complex pulse sequences. Simulation with SPROM can aid in analyzing experimental results from complex systems and identifying optimal parameters for experiments, thus saving substantial experimental time. Programmed with Visual C++, SPROM has an easy-to-use GUI and great extensibility. It will be freely available for those interested.

Acknowledgements

This work was partially supported by the NNSF of China under Grants 20573084, 10575085 and 10605019, and Project of Innovation Foundation of Xiamen University.

References

[1] H. Hagslatt, B. Jonsson, M. Nyden, O. Soderman, Predictions of pulsed field gradient NMR echo-decays for molecules diffusing in various restrictive geometries. Simulations of diffusion propagators based on a finite element method, J. Magn. Reson. 161 (2003) 138–147.
[2] C.L. Chin, F.W. Wehrli, S.N. Hwang, M. Takahashi, D.B. Hackney, Biexponential diffusion attenuation in the rat spinal cord: computer simulations based on anatomic images of axonal architecture, Magn. Reson. Med. 47 (2002) 455–460.
[3] M.H. Blees, The effect of finite duration of gradient pulses on the pulsed-field-gradient NMR method for studying restricted diffusion, J. Magn. Reson. A 109 (1994) 203–209.
[4] P. Allard, M. Helgstrand, T. Härd, A method for simulation of NOESY, ROESY, and off-resonance ROESY spectra, J. Magn. Reson. 129 (1997) 19–29.
[5] R.P.F. Kanters, B.W. Char, A.W. Addison, A computer-algebra application for the description of NMR experiments using the product-operator formalism, J. Magn. Reson. A 101 (1993) 23–29.
[6] M. Edén, Computer simulations in solid-state NMR.I. Spin dynamics theory, Concepts Magn. Reson. A 17 (2003) 117–154.
[7] É. Prost, S. Bourg, J.M. Nuzillard, Automatic first-order multiplet analysis in liquid-state NMR, C. R. Chimie 9 (2006) 498–502.
[8] H. Cheng, Q. Zhao, G.R. Duensing, W.A. Edelstein, D. Spencer, N. Browne, C. Saylor, M. Limkeman, SmartPhantom – an fMRI simulator, Magn. Reson. Imaging 24 (2006) 301–313.
[9] É. Prost, P. Sizun, M. Piotto, J.M. Nuzillard, A simple scheme for the design of solvent-suppression pulses, J. Magn. Reson. 159 (2002) 76–81.
[10] H.C. Torrey, Bloch equations with diffusion terms, Phys. Rev. 104 (1956) 563–565.
[11] P.L. De Sousa, D. Gounot, D. Grucker, Flow effects in long-range dipolar field MRI, J. Magn. Reson. 162 (2003) 356–363.
[12] L.A. Stables, R.P. Kennan, A.W. Anderson, J.C. Gore, Density matrix simulations of the effects of J coupling in spin echo and fast spin echo imaging, J. Magn. Reson. 140 (1999) 305–314.
[13] W.B. Blanton, BlochLib: a fast NMR C++ tool kit, J. Magn. Reson. 162 (2003) 269–283.
[14] M. Helgstrand, P. Allard, QSim, a program for NMR simulations, J. Biomol. NMR 30 (2004) 71–80.
[15] C.B. Cai, Z. Chen, S.H. Cai, J.H. Zhong, A simulation algorithm based on Bloch equations and product operator matrix: application to dipolar and scalar couplings, J. Magn. Reson. 172 (2005) 242–253.
[16] C.B. Cai, Z. Chen, S.H. Cai, L.P. Hwang, J.H. Zhong, Finite difference simulation of diffusion behaviors under inter- and intra-molecular multiple-quantum coherences in liquid NMR, Chem. Phys. Lett. 407 (2005) 438–443.
[17] Z. Chen, X.Q. Zhu, S.H. Cai, J.H. Zhong, Suppression of undesired peaks due to residual intermolecular dipolar interactions in liquid NMR, Chem. Phys. Lett. 417 (2006) 48–52.

[18] X.Q. Zhu, Z. Chen, S.H. Cai, J.H. Zhong, Selection of intra- or inter-molecular multiple-quantum coherences in NMR of highly polarized solution, Physica B 362 (2005) 286–294.
[19] X.Q. Zhu, Z. Chen, S.H. Cai, J.H. Zhong, Formation and identification of pure intermolecular zero-quantum coherence signal in liquid NMR, Chem. Phys. Lett. 421 (2006) 171–178.
[20] G. Deville, M. Bernier, J.M. Delrieux, NMR multiple echoes observed in solid 3H, Phys. Rev. B 19 (1979) 5666–5688.
[21] J. Jeener, A. Vlassenbroek, P. Broekaert, Unified derivation of the dipolar field and relaxation terms in the Bloch–Redfield equations of liquid NMR, J. Chem. Phys. 103 (1995) 1309–1332.
[22] S. Garrett-Roe, W.S. Warren, Numerical studies of intermolecular multiple quantum coherences: High-resolution NMR in inhomogeneous fields and contrast enhancement in MRI, J. Magn. Reson. 146 (2000) 1–13.
[23] M.L. Liu, X. Zhang, Multiple-quantum J-resolved NMR spectroscopy (MQ-JRES): Measurement of multiple-quantum relaxation rates and relative signs of spin coupling constants, J. Magn. Reson. 146 (2000) 277–282.
[24] P.T. Callaghan, A simple matrix formalism for spin echo analysis of restricted diffusion under generalized gradient waveforms, J. Magn. Reson. 129 (1997) 74–84.
[25] C.L. Chin, F.W. Wehrli, S.N. Hwang, D.L. Jaggard, D.B. Hackney, S.W. Wehrli, Feasibility of probing boundary morphology of structured materials by 2D NMR q-space imaging, J. Magn. Reson. 160 (2003) 20–25.
[26] J. Jeener, Macroscopic molecular diffusion in liquid NMR, revisited, Concepts Magn. Reson. 14 (2002) 79–88.
[27] S. Fichele, M.N. Woodhouse, P.D. Griffiths, E.J.R.V. Beek, J.M. Wild, Investigating He-3 diffusion NMR in the lungs using finite difference simulations and in vivo PGSE experiments, J. Magn. Reson. 167 (2004) 1–11.
[28] H. Cheng, F. Huang, Magnetic resonance imaging image intensity correction with extrapolation and adaptive smoothing, Magn. Reson. Med. 55 (2006) 959–966.
[29] W. Barros Jr., P.L. De Sousa, M. Engelsberg, Low field intermolecular double-quantum coherence imaging via the Overhauser effect, J. Magn. Reson. 165 (2003) 175–179.
[30] M. Engelsberg, W. Barros, F. Hallwass, Intermolecular double-quantum coherences in two-dimensional spectra of binary mixtures in solution. The role of diffusion, J. Chem. Phys. 120 (2004) 10659–10665.
[31] R. Bowtell, S. Gutteridge, C. Ramanathan, Imaging the long-range dipolar field in structured liquid state samples, J. Magn. Reson. 150 (2001) 147–155.